Quaternary Research 73 (2010) 425–438

Contents lists available at ScienceDirect

Quaternary Research

journal homepage: www.elsevier.com/locate/yqres

Timing and distribution of alluvial fan sedimentation in response to strengthening of late Holocene ENSO variability in the Sonoran Desert, southwestern Arizona, USA

Steven N. Bacon *, Eric V. McDonald, Todd G. Caldwell, Graham K. Dalldorf

Desert Research Institute, Division of Earth and Ecosystem Sciences, Reno, NV 89512, USA

ARTICLE INFO

Article history:
Received 5 August 2009
Available online 4 March 2010

Keywords:
Late Holocene
Alluvial fan
Desert soils
Sonoran Desert
Geomorphology
Paleoclimatology
ENSO variability

ABSTRACT

The integration of geomorphic mapping, soil stratigraphy, and radiocarbon dating of alluvial deposits offers insight to the timing, magnitude, and paleoclimatic context of Holocene fan sedimentation near Yuma, Arizona. Mapping of 3400 km^2 indicates about 10% of the area aggraded in the late Holocene and formed regionally extensive alluvial fan and alluvial plain cut-and-fill terraces. Fan deposits have weakly developed gravelly soils and yielded a date of 3200–2950 cal yr BP from carbonized wood. Alluvial plain deposits have weakly developed buried sandy soils and provided a date of 2460–2300 cal yr BP from a terrestrial snail shell. Precipitation records were analyzed to form historical analogues to the late Holocene aggradation and to consider the role of climatic variability and extreme hydrologic events as drivers of the sedimentation. The historical precipitation record indicates numerous above-average events correlated to the Southern Oscillation Index (SOI) in the region, but lacks any significant reactivation of alluvial fan surfaces. The timing of aggradation from 3200 to 2300 cal yr BP correlates well with other paleoclimatic proxy records in the southwestern U.S. and eastern Pacific region, which indicate an intensification of the El Niño-Southern Oscillation (ENSO) climatic pattern and rapid climate change during this period.

Introduction

Quantifying the timing and magnitude of past alluvial sedimentation in the arid southwestern U.S. offers insight to the hydrologic variability of the region and provides data for paleoclimatic models. Most studies with a significant component of surficial geomorphic mapping for paleoclimatic inferences are performed over areas of tens to hundreds of km^2. Many of these studies correlate similar-aged episodes of alluvial aggradation that span several drainage basins to infer the physical linkages between climatic forcing and system response over a much broader region (e.g., McFadden et al., 1989). The majority of these types of studies have focused on dating Pleistocene–Holocene transition alluvial deposits to understand climate change (Wells et al., 1987; Bull, 1991; Waters and Haynes, 2001; McDonald et al., 2003). By comparison, the application of alluvial fans as paleoclimatic proxy evidence to determine the frequency and magnitude of past changes and activity of Holocene global climatic circulation patterns has been underutilized in most studies (Donders et al., 2008). Most geologic-based studies in the western U.S. that aim to understand the connection between geomorphic change and Holocene climate variability and moisture sources have been focused on lake-level and playa lake inundation records (e.g., Enzel et al., 1989; Scuderi et al., 2010). Yet, the timing and response of alluvial fan systems to an increase in frequency and intensity of the El Niño Southern Oscillation (ENSO) climatic pattern at the beginning of the late Holocene (Liu et al., 2000) are not well-documented in the southwestern U.S.

Widespread alluvial fan deposits of late Holocene age have been documented in the Sonoran and Mojave Deserts. In particular, regional alluvial fan deposits mapped as unit Q3c by Bull (1991) were generally estimated to be of late Holocene age based on soil-geomorphic characteristics in the lower Colorado River region of southern Arizona. Most of these fan deposits grade to large stream systems that contain an extensive late Holocene alluvial record (Waters, 2008). Similar geomorphic surfaces and deposits are also present in the Mojave Desert indicating significant periods of Holocene fan aggradation in the form of widespread fill terraces and coalescing distal fan lobes (McDonald et al., 2003; Mahan et al., 2007; Miller et al., 2010). These chronologies also show that alluvial sediments aggraded in the late Holocene at scales not represented in the historical record.

This study uses small- and large-scale geomorphic mapping, field and laboratory characterization of soils, as well as ^{14}C dating of alluvial deposits to show the timing and distribution of sedimentation in southwestern Arizona that coincides with a period of greater precipitation in the region. The goals of this paper are three-fold: (1) to show soil-geomorphic supporting evidence and ^{14}C-based age constraints for the previously undated episode of extensive alluvial fan aggradation in southwestern Arizona; (2) to identify the climatic causes for this aggradation by reviewing historical climatic records to

* Corresponding author. Desert Research Institute, Division of Earth and Ecosystem Sciences, 2215 Raggio Parkway, Reno, NV 89512, USA.

0033-5894/$ – see front matter © 2010 University of Washington. Published by Elsevier Inc. All rights reserved.
doi:10.1016/j.yqres.2010.01.004

develop modern analogues to the late Holocene sedimentation; and (3) to demonstrate how the late Holocene aggradation near Yuma correlates well with other geomorphic and stratigraphic records that are thought to be associated with intensified ENSO cycles.

Study area

Geomorphic mapping and soil stratigraphic investigations were performed on the U.S. Army Yuma Proving Ground (YPG) north of Yuma in southwestern Arizona (Fig. 1). The study area is within the western Sonoran Desert having an arid climate with a mean annual precipitation measured at YPG headquarters of 93 mm (32°59′N, 114°23′W; elev. 97 m; period of record AD 1958–2007). The region has many physiographic features common to the southern Basin and Range and lower Colorado River regions, which has minimal neotectonic activity. The mountain ranges are of moderate to low relief and composed mostly of Cretaceous- and Tertiary-age granitic and volcanic rocks, and lesser sedimentary rocks (Richard et al., 2000). The mountains ranges separate broad and low-gradient and incised alluvial slopes or piedmonts that have graded to different base levels of the ancestral positions of the Colorado and Gila Rivers (e.g., Wilshire and Reneau, 1992). The piedmont in the study area is dominated by a sequence of middle to late Pleistocene alluvial fans that exhibit well-developed and varnished desert pavement surfaces, with less extensive inset Holocene alluvial fan and alluvial-plain terraces and active washes (Lashlee et al., 2001; Nichols et al., 2006) (Fig. 1).

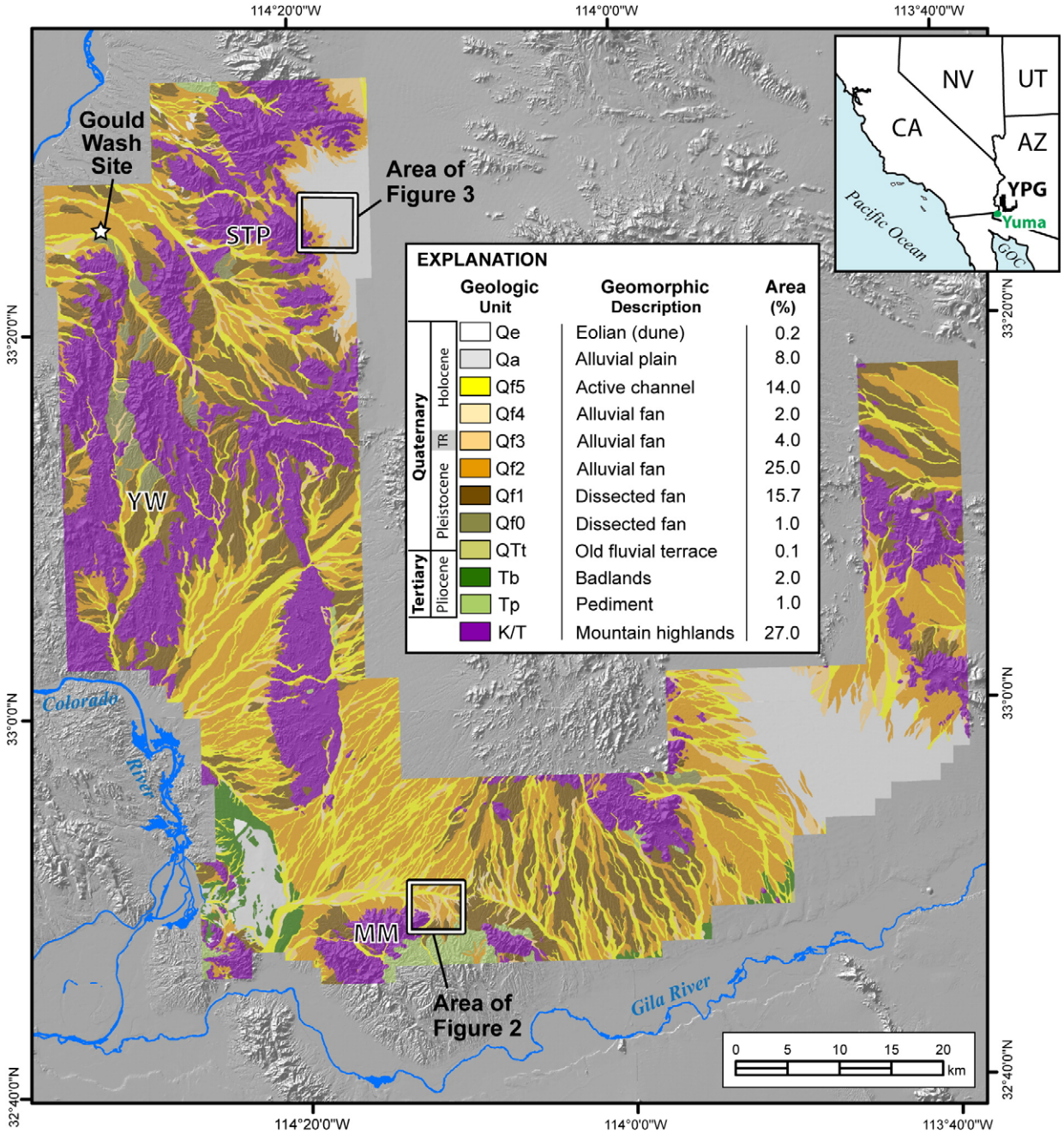

Figure 1. Geomorphic map of landforms mapped at scales between 1:24,000 and 1:50,000 within YPG. Topographic data are based on U.S. Geological Survey 10 m national elevation data. The drainages of the Colorado and Gila Rivers are shown in blue. The white boxes indicate the locations of the Muggins Mountains and South Trigo Peak study sites on Figures 2 and 3, respectively, and the star denotes the location of the Gould Wash study site. STP, South Trigo Peak; MM, Muggins Mountains; YW, Yuma Wash; TR, Pleistocene–Holocene transition; GOC, Gulf of California.

https://doi.org/10.1016/j.yqres.2010.01.004 Published online by Cambridge University Press

Methods

Geomorphic mapping

Mapping involved classifying the landscape into geomorphic units within all of the 3400 km^2 of YPG. The Natural Resources Conservation Service 1:24,000-scale soil map was used as an initial base map (Cochran, 1991). We modified and converted the soil map units to geomorphic map units and added additional units, based on 1- and 5-m resolution IKONOS satellite imagery and 10-m resolution digital elevation model at a scale of 1:50,000 using GIS software (Fig. 1). Large-scale (1:5000-scale) mapping based on 1-m resolution IKONOS satellite imagery was completed at two sites referred to as Muggins Mountains and South Trigo Peak A located in southern and northern YPG, respectively (Figs. 1–3). Landforms were classified into geomorphic units following a modified categorization scheme of Peterson (1981). Geomorphic units were then assigned relative surface ages based on cross-cutting relations, surface morphology, and soil characteristics (e.g., Bull, 1991), and given correlative alluvial-fan ages based on numerical ages where applicable (Nichols et al., 2006). Map unit descriptors are as follows: Quaternary alluvial fan (f) and alluvial-plain (a) surfaces are labeled Qf0 to Qf5 and Qa1 to Qa3, from oldest to youngest, respectively.

Numerical age-control and soil investigation

Four ^{14}C dates are used to establish age control at sites with soil-geomorphic information (Table 1). Radiocarbon dates (^{14}C yr BP) have been calibrated to calendar years before present (cal yr BP) using the CALIB v. 5.0.2 program (Stuiver and Reimer, 1993) with the INTCAL04 data set (Reimer et al., 2004). Soil profile data from two additional sites in YPG, referred to as Gould Wash and South Trigo Peak B (Figs. 1 and 3), which do not have numerical age control, are correlated to sites with ^{14}C dates based on similar surface morphology and soil-geomorphic characteristics (McFadden et al., 1989; McDonald et al., 2003). Numerous trenches were placed on late Holocene surfaces across the study area. The late Holocene soils presented in this paper are the most representative and the sites of ^{14}C datable materials. Soil morphology was described using standard methods and modified using soil-geomorphic information (Soil Survey Staff, 1998; Birkeland, 1999). A representative soil sample was collected from each genetic soil horizon identified in the field. Soil samples were oven dried at 105°C for 24 h and the gravel fraction (>2 mm) removed using a No. 10 sieve. All laboratory analysis, including calcium carbonate ($CaCO_3$) and soluble salt (NaCl or $CaSO_4 \cdot 2H_2O$) contents, were preformed on the fine earth fraction (<2 mm).

Results

Small-scale geomorphic mapping

Twelve geomorphic units were identified at a scale of 1:50,000 in an area of 3400 km ^{2} (Fig. 1). The geomorphic units exhibit a diverse range of surface, soil, and morphometric characteristics that have been described in detail by Bacon et al. (2008). Mapping shows that ~70% of the area consists of alluvial geomorphic units. The remaining

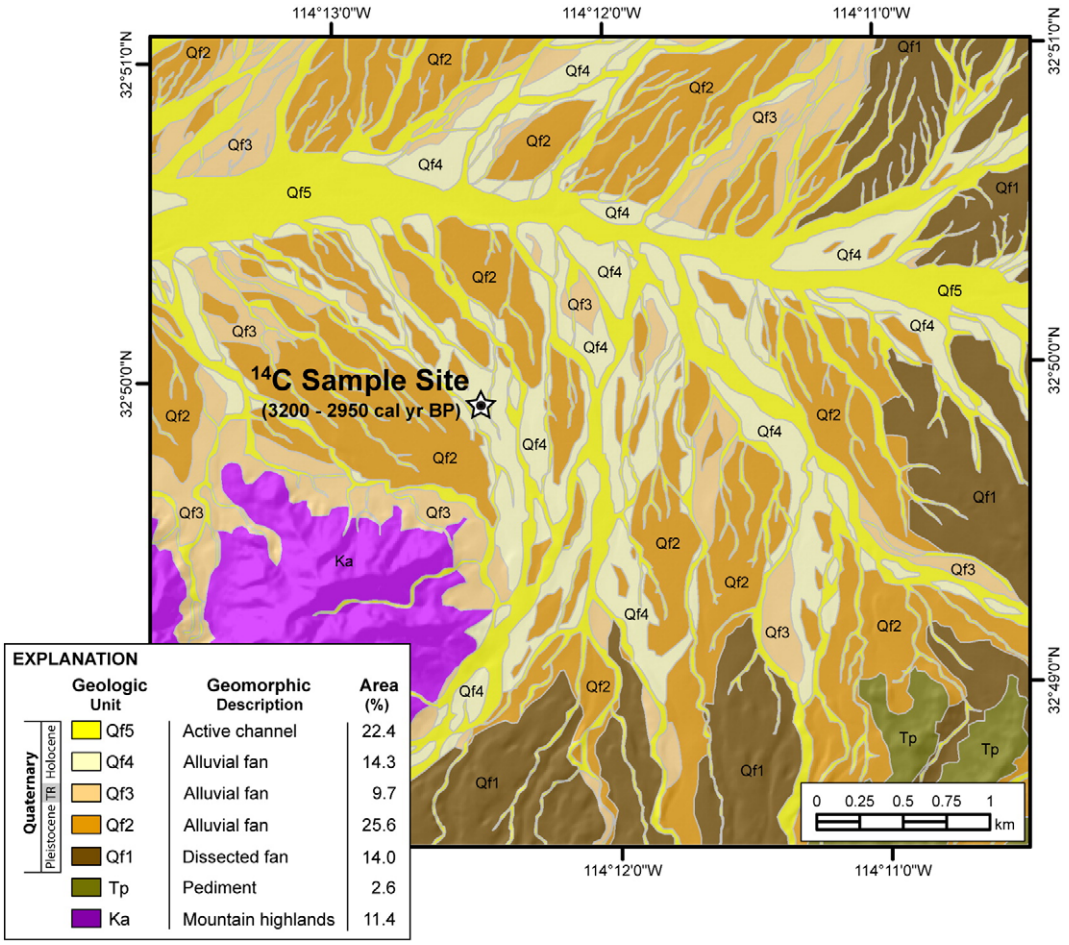

Figure 2. Geomorphic map of the Muggins Mountains study site showing the distribution and percent area of individual map units. Map unit boundaries were delineated based on geomorphic surface characteristics and cross-cutting relations using 1-m resolution IKONOS satellite imagery. The soil trench location and ^{14}C sample site on the Qf4 unit are shown with a star. TR, Pleistocene–Holocene transition.

https://doi.org/10.1016/j.yqres.2010.01.004 Published online by Cambridge University Press

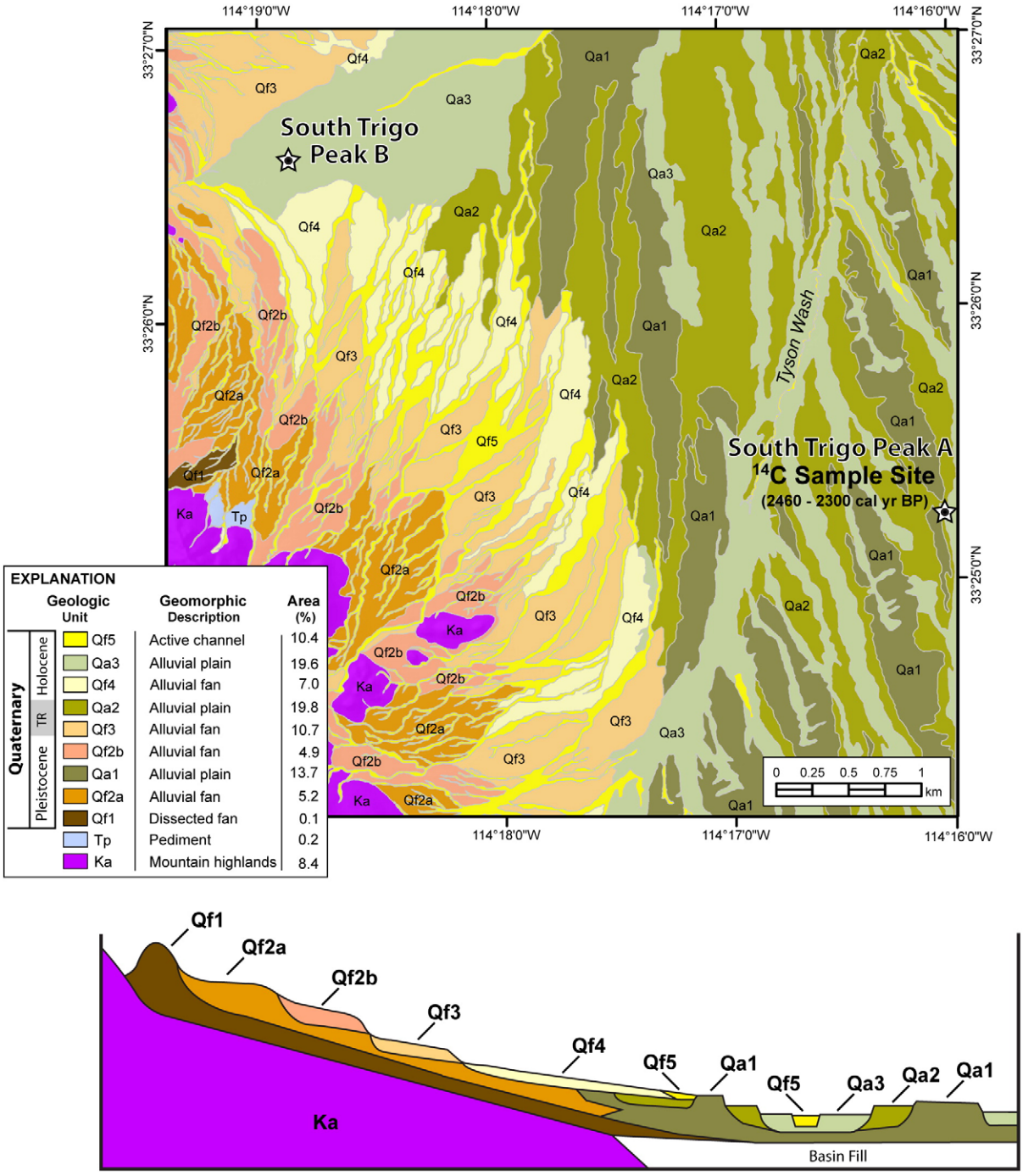

Figure 3. Geomorphic map of South Trigo Peak A and B study sites and schematic cross section showing the distribution and percent area of individual map units. Map unit boundaries were delineated based on geomorphic surface characteristics and cross-cutting relations using 1-m resolution IKONOS satellite imagery. The soil trench location and ^{14}C sample site on the Qa3 unit are shown with a star. TR, Pleistocene–Holocene transition.

~30% of non-alluvial units are mountain highlands composed of Cretaceous and Tertiary-age bedrock (K/T), pediment landforms (Tp) developed on bedrock, as well as badland landforms (Tb) composed of the Mio-Pliocene Bouse Formation (e.g., House et al., 2008). In addition, "old" fluvial terraces (QTt) equivalent to the Plio-Pleistocene (3–0.8 Ma) river deposits of Olmsted (1972) and active eolian dunes (Qe) were also mapped (Fig. 1). The two oldest alluvial fan units (Qf0 and Qf1) are extremely to moderately dissected, display ballena topography, and comprise 1.0% and ~16.0% of the map area, respectively. The most prevalent unit is late Pleistocene alluvial fan (Qf2), which comprises ~25% of the map area and exhibits strongly developed desert pavement and varnished surfaces (McAuliffe and McDonald, 2006). The Qf2 unit likely was deposited from ~140 to 70 ka (Nichols et al., 2006). Inset to the Qf2 unit are three alluvial surfaces that include 4.0% Pleistocene–Holocene transition alluvial fan (Qf3) that exhibits strongly to moderately developed desert pavement and varnished surfaces, 2.0% late Holocene alluvial fan (Qf4) with poorly developed desert pavement and incipient varnish, and 14.0% active channel (Qf5). The remaining 8.0% of the area within YPG consists of alluvial plain terraces (Qa) (Fig. 1). This unit consists primarily of late Holocene deposits but includes strongly developed desert pavement and varnished surfaces of likely latest Pleistocene age that are not mappable at the scale shown, but are described in the following large-scale geomorphic mapping section.

https://doi.org/10.1016/j.yqres.2010.01.004 Published online by Cambridge University Press

Table 1
Radiocarbon dating results and calibrations.

Site	Material dated[a]	Lab number[b]	Date (^{14}C yr BP)	δ^{13}/δ^{12} (‰)	Calendar age[c](cal yr BP)
Muggins Mountains					
(Unit Qf4)	Carbonized wood, Ironwood *(Olneya tesota)*	Beta-217306	2880 ± 40	−32.4	3160–3090; **3080–2920**; 2910–2880
	Carbonized wood, Ironwood *(Olneya tesota)*	Beta-217307	3000 ± 40	−32.3	3340–3070
	Carbonized wood, Ironwood *(Olneya tesota)*	Beta-217308	2850 ± 40	−30.9	3140–3130; **3080–2850**
		Mean	2910 ± 40	−31.9	3200–2950
South Trigo Peak A					
(Unit Qa3)	Snail shell (*Lymnea* sp. or *Succinea* sp.)	Beta-232710	2320 ± 40	−6.0	**2460–2300**; 2240–2180; 2170–2160

[a] Accelerator mass spectrometry (AMS) analysis was performed on samples.
[b] Beta = Beta Analytic, Inc., Miami, Florida.
[c] Radiocarbon date is calibrated at 2 σ using CALIB v 5.0.2 program (Stuiver and Reimer, 1993) with the INTCAL04 data set (Reimer et al., 2004); bold range includes the *y*-intercept and has the highest probability distribution.

Large-scale geomorphic mapping and late Holocene soils

Muggins Mountains site

Areas of large-scale (1:5000) mapping were chosen because dateable materials were found in soil trenches and the alluvial geomorphology is representative of the study area. One of the large-scale map areas is in southwestern YPG near Muggins Mountains (Fig. 1). Geomorphic mapping in an area of 25 km^2 at this site shows ~15% of the surrounding Quaternary alluvium is late Holocene Qf4 unit (Fig. 2). The Qf4 unit is inset to both Qf2 and Qf3 units, respectively, and has gently sloping surface gradients that parallel active washes positioned ~1.5 m lower. The Qf4 surfaces also have moderate bar-and-swale microtopography and weakly developed desert pavement with incipient coatings of light brown varnish on clasts (Fig. 4a). A trench excavated into a Qf4 surface exposed normally graded and moderately to well stratified pebble-gravel braided stream deposits that were capped by a ~3-cm-thick wind blown silt layer referred to as an Av (vesicular) horizon (McFadden et al., 1998) (Fig. 2). The weakly developed soil has an Av/Bw/Cky profile, an extremely gravelly texture that lacks soil structure, and contains secondary calcium carbonate and gypsum (Table 2; Fig. 5a). There were no observable erosional boundaries or buried soils at the site. The location and presence of the ^{14}C sample defines two episodes of aggradation that were deposited close in time (Fig. 5a). Secondary

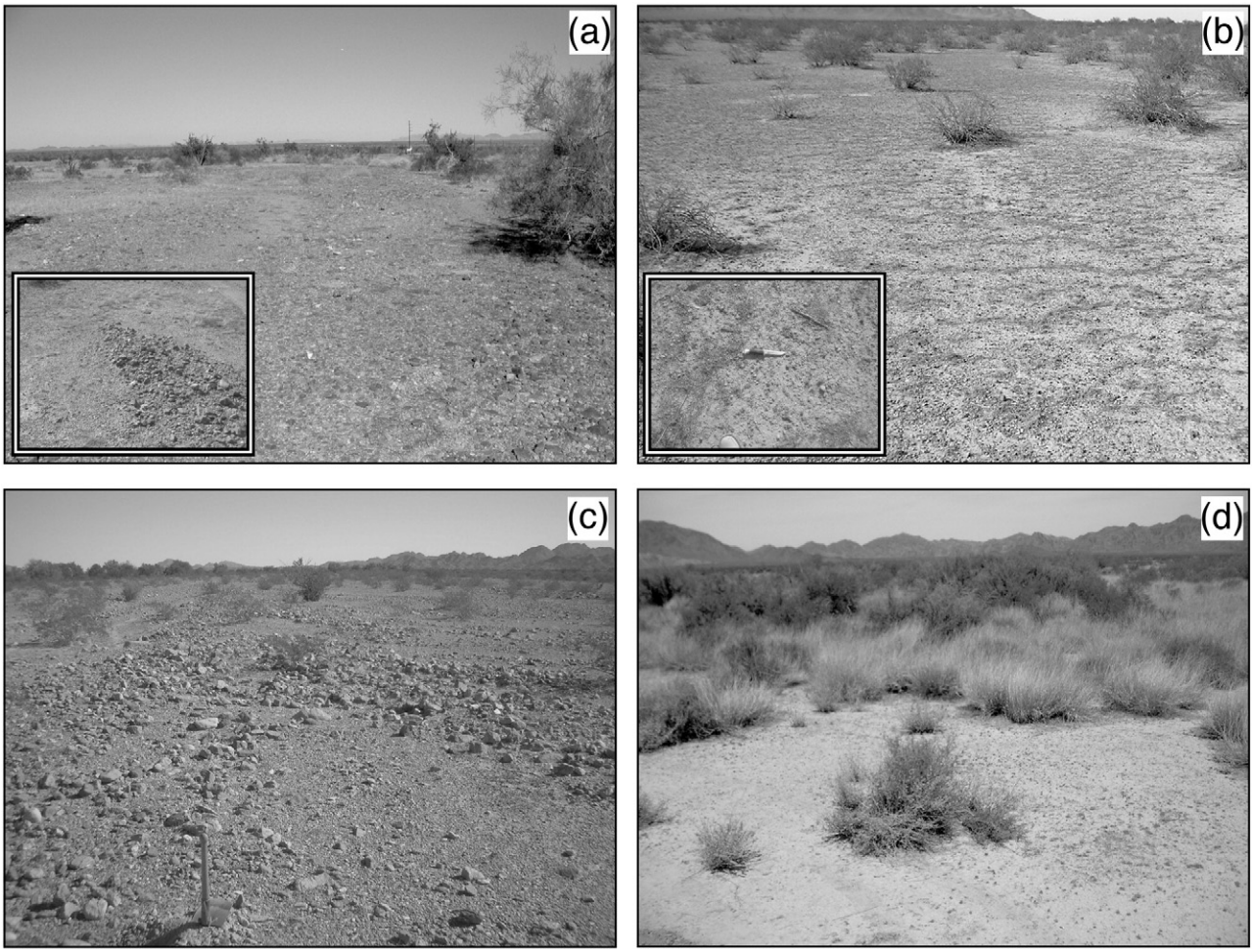

Figure 4. Field photos of the different characteristics of alluvial fan and plain surfaces in the study. (a) Qf4 surface at Muggins Mountains site that exhibits moderate bar-and-swale microtopography; inset photo is close-up of gravelly bar. (b) Qa3 surface at South Trigo Peak A site; inset photo is close-up of surface, knife for scale. (c) Qf4 surface at the Gould Wash site that has moderate bar-and-swale microtopography; shovel for scale. (d) Qa3 surface at South Trigo Peak B site that has a lag pavement with no varnish on clasts.

https://doi.org/10.1016/j.yqres.2010.01.004 Published online by Cambridge University Press

Table 2
Summary of morphological and textural characteristics of soils developed on late Holocene alluvial fan and plain deposits within the Sonoran Desert near Yuma, Arizona.

Site	Horizon[a]	Depth (cm)	Color dry matrix	Texture[a]	Structure[a]	Consistency[a] dry matrix	Particle size (<2 mm)[b]			$CaCO_3$[c] (%)	Salinity[d] (mg/g)	Deposit age
							Sand	Silt	Clay			
Muggins Mountains	Avk	0–3	10YR 8/4	vgrcl	1mpr/1msbk	so	45	28	27	5.8	0.30	Late Holocene
Lat: 32°49.86′N	Bwk	3–9	10YR 7/4	xgrsl	m/1fsbk	so	78	13	9	6.1	0.19	" "
Long: 114°12.42′W	Ck1	9–23	10YR 6/4	xgrls	s/g	lo	78	16	6	3.7	0.18	" "
El: 196 m	Ck2	23–33	10YR 6/4	grls	m	so/lo	78	17	5	3.2	0.14	" "
	Cky1	33–80	10YR 5/4	xgrs	sg	lo	92	5	3	3.8	3.33	" "
	Cky2	80–107+	10YR 5/4	xgrs	m/sg	so/sh	95	3	2	2.0	1.04	" "
South Trigo Peak A	AC	0–6	10YR 6/4	l	2-3thpl/2msbk	so	34	49	17	7.8	0.94	Recent to
Lat: 33°25.26′N	C	6–18	10YR 7/4	vgrl	sg/m	so/lo	71	17	12	12.0	1.26	Latest Holocene
Long: 114°16.02′W	$Bwkb_1$	18–55	10YR 5/8	l	1msbk/m	sh/so	36	41	23	18.0	5.54	Late Holocene
El: 368 m	$Bwk1b_2$	55–76	10YR 5/6	l	1msbk	sh	39	40	21	23.5	4.57	N.A.
	$Bwk2b_2$	76–114	10YR 5/6	grl	1msbk	sh	51	37	12	13.8	3.80	N.A.
	$BCkb_2$	114–138	10YR 6/6	sl	m	sh/so	59	31	10	8.3	3.01	N.A.
	$Bwkb_3$	138–173+	5YR 5/6	grl	1msbk/m	h/sh	41	44	15	26.9	4.22	N.A.
Gould Wash	Avk	0–3	10YR 8/4	l	2msbk	so	52	32	15	4.0	0.39	Late Holocene
Lat: 33°25.32′N	Bwk	3–8	10YR 6/4	vgrsl	1fsbk	so/sh	61	27	12	5.4	0.26	" "
Long: 114°31.89′W	Ck	8–22	10YR 6/4	xgrls	sg	lo	85	13	3	4.0	0.60	" "
El: 185 m	Cky1	22–46	10YR 6/4	xgrs	sg	lo	91	8	2	3.6	4.62	" "
	Cky2	46–71	10YR 5/4	xgrs	Sg	lo	91	7	2	2.7	3.89	" "
	Cky3	71–102	10YR 5/4	xgrls	sg	lo	75	21	4	4.2	4.04	" "
	Ck	102–124+	10YR 5/4	xgrls	sg/m	lo	82	13	5	3.6	2.54	" "
South Trigo Peak B	AC	0–6	10YR 8/4	l	2-3tkpl/2msbk	sh	45	43	12	9.8	1.06	Recent to
Lat: 33°26.82′N	C1	6–15	10YR 8/4	l	1-2tkpl/1-2fabk	sh/so	50	39	11	7.0	0.52	Latest Holocene
Long: 114°18.54′W	C2	15–29	10YR 7/4	sl	m	so	78	14	8	5.0	0.39	" "
El: 358 m	$Bwkb_1$	29–53	7.5YR 6/6	sl	1mpr/1msbk	vh/h	68	19	13	9.2	0.43	Late Holocene
	$Bwkyb_1$	53–74	7.5YR 6/8	sl	1msbk	sh	69	19	12	12.3	0.53	Late Holocene
	$Btkb_2$	74–107	5YR 5/4	ls	1-2msbk	sh/h	86	9	5	33.1	0.47	N.A.
	$Btky1b_2$	107–134	5YR 5/4	ls	1-2msbk	vh/h	84	10	6	51.5	0.59	N.A.
	$Btky2b_2$	134–154+	5YR 5/8	sl	m	vh	75	17	8	38.0	0.66	N.A.

Note. Latitude and longitude in WGS84 datum; Elevation in meters above mean sea level; N.A. = no numerical age.
[a] Notations from Soil Survey Staff (1998), Schoeneberger et al. (2002), and Birkeland (1999).
[b] Particle size distribution measured using the laser light-scattering method of Gee and Or (2002) for all soils, except for Muggins Mountains site where the pipette method after removal of calcium carbonate and soluable salts by the sodium acetate digestion method was used.
[c] Calcium carbonate content measured using the Chittick apparatus method of Dreimanis (1962) and Machette (1985).
[d] Salinity of total soluable salts based on electrical conductivity (EC) of aqueous soil extracts using a soil-water extract of 1:5 (Rhoades, 1996).

calcium carbonate decreases with depth from ~6 to 2% wt., with stage I to I+ carbonate morphology (Table 2).

Numerical age control at the site is from a well-preserved 5 cm in length and 2. 5 cm in diameter carbonized woody stem of Ironwood (*Olneya tesota*). The sample was recovered from a depth of 75 cm at a clear and conformable boundary between upper soil units (Ck1-Cky1) and lower soil unit (Cky2). It yielded three AMS dates of 2880± 40, 3000± 40, and 2850±40 ^{14}C yr BP [3340 to 2850 cal yr BP] having a mean date of 2910± 40 ^{14}C yr BP [3200–2950 cal yr BP] (Table 1; Fig. 5a). The large intact size and degree of preservation of the wood combined with its soil-geomorphic context suggest that reworking of the woody material much older than the alluvial episode is unlikely. We interpret the ^{14}C age of the wood as a maximum estimate of its time of death, but it likely is reasonably close to the age of emplacement of the deposits.

South Trigo Peak A site

We mapped and investigated similar aged alluvial features near South Trigo Peak in northwestern YPG, located about 70 km north of the Muggins Mountains site (Fig. 1). Large-scale (1:5000) geomorphic mapping in an area of 30 km ^{2} at the South Trigo Peak A site shows the distribution of late Holocene Qa3 and equivalent Qf4 units to include ~20% and 7% of the surrounding Quaternary alluvium, respectively. The Qf4 units, as well as other alluvial units observed along the piedmont have surface and soil characteristics that are similar to the corresponding mapped units described at the Muggins Mountains site. The South Trigo Peak site has a broad axial plain (Tyson Wash) that exhibits a series of north-northwest trending alluvial-plain surfaces of different ages (units: Qa1-Qa3), which are not present at the Muggins Mountains site (Fig. 3). The oldest Qa1 unit exhibits a strongly developed desert pavement and varnished clasts having surface characteristics similar to the Qf2b unit, but with much smaller surface clasts, and is probably late Pleistocene in age. The Qa2 unit has strongly to moderately developed desert pavement and varnished clasts similar to the Qf3 unit, and is probably latest Pleistocene to early Holocene in age.

The late Holocene Qa3 surfaces are positioned 0.5 to 1. 0 m above active washes. These surfaces are moderately to sparsely vegetated with Creosote bush (*Larrea tridentata*), have moderate bar-and-swale microtopography with a lag pavement and no varnish on clasts, and appear to be equivalent to the Qf4 unit (Fig. 4b). A trench excavated into the Qa3 surface exposed a sequence of normally graded and poorly to moderately stratified sandy-pebble channel and flood deposits. The deposits have a very weak surface soil and three weakly developed buried soils consisting of alternating loam and gravelly textures and moderate secondary calcium carbonate accumulation (Table 2; Fig. 5b). The buried ~37-cm-thick late Holocene soil unit at depths between 18 and 55 cm includes secondary carbonate content of 18% wt., a structure ranging from structureless to medium subangular blocky, and a slightly hard to soft consistency (Table 2).

Numerical age control at the site is from a moderately preserved, 0.75 cm diameter shell fragment that was recovered from a depth of 50 cm and yielded an AMS date of 2320± 40 ^{14}C yr BP [2460–2300 cal yr BP] (Table 1; Fig. 5b). The portion of the recovered shell fragment appears to be either an aquatic (*Lymnea* sp.) or semi-aquatic (*Succinea* sp.) terrestrial snail. It is likely that the shell fragment is a Succinid because it was recovered from deposits that represent an ephemeral depositional environment. Semi-aquatic snails generally favor moist, well-vegetated areas along the edges of marshes and streams, and have been shown to sustain themselves for periods of relatively dry

https://doi.org/10.1016/j.yqres.2010.01.004 Published online by Cambridge University Press

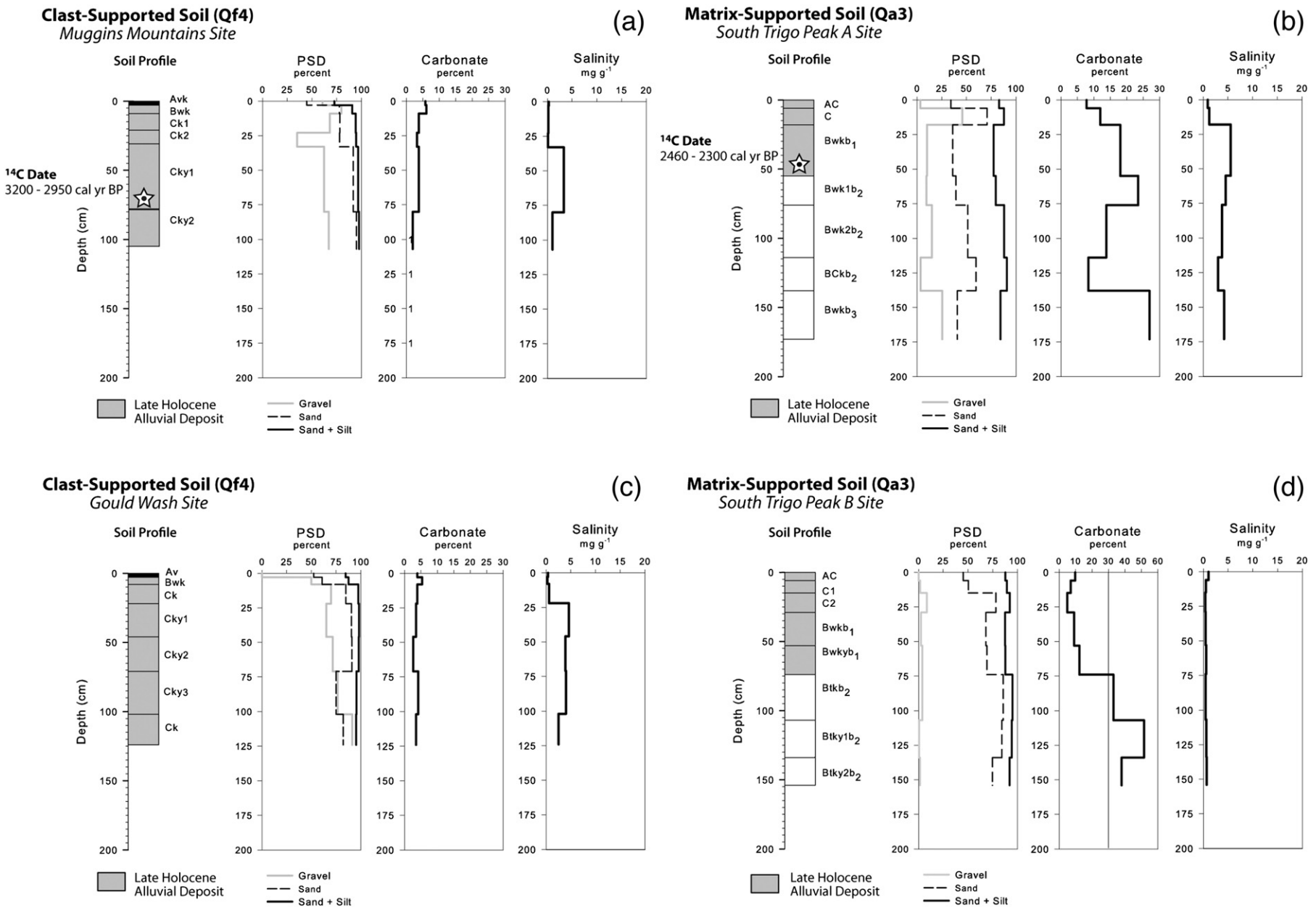

Figure 5. Soil profile designations, down-depth particle size distributions, and carbonate and salinity contents for clast-supported Qf4 soils and matrix-supported Qa3 soils. The locations of ^{14}C samples at Muggins Mountains and South Trigo Peak A sites are shown with stars. Horizons colored gray in soil profiles signify dated and correlated late Holocene deposits.

conditions (Bequaert and Miller, 1973). Many varieties of aquatic mollusk grow their shells in waters with an initial ^{14}C deficiency and as a result, yield artificially older ^{14}C ages (Brennan and Quade, 1997), but some taxa of semi-aquatic snails, such as Succinids, provide reliable ^{14}C ages (Pigati et al., 2004). Therefore, we interpret the age of the snail shell as a maximum estimate of its time of death, thereby providing a maximum age constraint for the deposit. The ^{14}C sample was located ~5 cm above an erosional boundary and constrains the age for buried soil unit ($Bwkb_1$) as late Holocene.

Correlated soil-geomorphic sites

Gould Wash site

Soil stratigraphy and geomorphic setting at the Gould Wash site support correlation between the dated Muggins Mountains site and similar fan units at the South Trigo Peak A site. Collectively, the sites show regional distribution of alluvial fan deposits of late Holocene age across the entire study area (Fig. 1). The Gould Wash site exhibits another example of late Holocene Qf4 deposits and soils in YPG that are typically inset to Qf2 and Qf3 units. The close proximity of the site to the Colorado River controls surface gradients of alluvial surfaces in the area, where the Qf4 unit is more gently sloping compared to active washes that are positioned 1.5 to 2. 0 m lower. The surface is sparsely vegetated with *L. tridentata* and exhibits moderate bar-and-swale microtopography and weakly developed desert pavement with incipient coatings of light brown varnish on clasts (Fig. 4c). The Qf4 deposit consists of a stratified sequence of clast supported, moderately to well-sorted pebble-gravel braided stream deposits that are capped by a ~3-cm-thick Av horizon. The weakly developed soil has a general Av/Bwk/Cky profile, an extremely gravelly texture that lacks soil structure, and has weak carbonate and gypsum accumulation (Table 2; Fig. 5c). The boundary between upper soil units (Bk-Cky1) and lower soil units (Cky2 and Ck) represents two episodes of aggradation that were deposited close in time (Fig. 5c). Carbonate content ranges from ~3 to 5% wt., with stage I to I+ carbonate morphology (Table 2).

South Trigo Peak B site

Soil stratigraphy and geomorphic setting of the South Trigo Peak B site also support correlation between the dated South Trigo Peak A site, as well as representing a lower-energy depositional environment. The South Trigo Peak B site differs from the South Trigo Peak A site in that it is fairly far from active channels, and fine-grained sediment accumulates in depressions versus channel through flow during flood events. The South Trigo Peak B site is ~4. 5 km northwest of the South Trigo Peak A site and is situated within a broad and gently sloping axial plain consisting of Qa3 surfaces (Fig. 3). The surfaces are moderately to densely vegetated with Mesquite trees (*Prosopis* sp.) and Galetta grass (*Pleuraphis rigida*) in depressions, exhibits a lag pavement with no varnish on clasts, and is positioned ~0.5 to 1. 0 m above active channels (Fig. 4d). The Qa3 unit has a sequence of poorly stratified to massive sand and silt deposits. The deposits have a soil profile that includes alternating loamy sand to silt loam textures, massive to medium angular blocky soil structures, and low calcium carbonate and gypsum accumulation. Two erosional boundaries were identified that define buried soils at the site (Table 2; Fig. 5d). The buried ~45-cm-thick late Holocene Bwk soil unit at a depth from 29 to 74 cm includes a carbonate content of ~9–12% wt., a structure that ranges from medium prismatic to medium subangular blocky, and a slightly hard to very hard consistency (Table 2).

Late Holocene soil development

The soils at the Muggins Mountains and Gould Wash sites are developed on moderately stratified and well-sorted coarse-grained fan deposits, whereas the soils at the South Trigo Peak A and B sites are developed on poorly stratified and poorly sorted fine-grained alluvial plain deposits. The parent material at the sites generally consists of mixed lithologies of granitic rock and volcanic tuff and basalt, with minor amounts of metasedimentary rock. The degree of soil development at the Muggins Mesa and Gould Wash sites is similar, with soil profiles consisting of thin Av and Bw horizons over a thick sequence of Cky horizons. The characteristics of these gravelly soils exhibit traits that are typical of aridic soils having significant amounts of eolian dust-derived secondary silt, clay, and carbonate or gypsum that have been incorporated into the soil (e.g., Reheis et al., 1995). The degree of soil development is also similar between the South Trigo Peak A and B sites, consisting of a sequence of weakly developed buried soils. It appears that soil development at the South Trigo Peak sites is also controlled by a degree of dust flux, but mostly by leaching depth and the incorporation of previously weathered sediments into the deposits because of their fine-grained properties and flood-prone depositional settings.

The coarse-grained Qf4 soils and geomorphic surfaces have similar pedologic and surface feature characteristics to the aggradation event (Q3c) of Bull (1991) in the lower Colorado River region, with an estimated age of 2 to 4 ka based on weakly developed soils and surface cobbles with incipient coatings of light brown varnish. The numerical age constraints for the coarse-grained Qf4 soils obtained in this study fall within this age range. Furthermore, the Qf4 deposits in YPG have notably similar surface characteristics and degree of soil development to other gravelly fan deposits of late Holocene age in the Mojave Desert (Wells et al., 1987; Reheis et al., 1995; McDonald et al., 2003).

Discussion

Distribution and processes of late Holocene alluvial sedimentation

The majority of late Holocene Qf4 deposits in YPG form a regional cut-and-fill sequence that consists of well-sorted gravels, typical of fluvial-dominated braided stream systems. A similar cut-and-fill sequence applies to the Qa3 deposits, but is notably different because it includes moderately- to poorly-sorted, stratified sands and silts and lesser gravels, representative of flood prone and palustrine depositional environments common to distal piedmont locations. The Qf4 and Qa3 deposits are both inset into older deposits and are preserved on the edges of active channels and washes. Preservation of Qf4 surfaces at the Muggins Mountains and Gould Wash sites appears to have been controlled in part by near-field changes in base level of the Colorado and Gila Rivers based on different magnitudes of incision at the sites (Figs. 1 and 2). There are, however, notable differences in fan development and the distribution of Qf4 surfaces along the piedmont at the South Trigo Peak site. Here, local areas of the piedmont have formed from coalescing fan lobes graded to the broad and low-gradient Tyson Wash axial drainage system. The Qa1–Qa3 surfaces within Tyson Wash appear to have been preserved by subtle down-cutting controlled by far-field changes in base level of the Colorado River during times with little aggradation (Figs. 1 and 3).

Processes associated with the morphometry of the piedmont slopes in YPG are largely influenced by sediment-deficient stream discharge from sub-basins during times of relative aridity rather than processes associated with structural-controlled uplift of piedmont slopes because the study area is tectonically quiescent. Variation in sediment discharge has promoted entrenchment of the older fan deposits at the Muggins Mountains and Gould Wash sites and telescoping models of sedimentation at the South Trigo Peak site (e.g., Ritter et al., 2000) (Fig. 3). Frequent and intense precipitation events and floods could have promoted an increase in stream discharge and sediment load from sub-basins, as well as the reworking of stored sediment along the boundaries of washes promoting aggradation of the Qf4 and Qa3 deposits. These relations are supported by Clapp et al. (2002), who used ^{10}Be and ^{26}Al in sediment samples to determine sediment generation rates from Yuma

https://doi.org/10.1016/j.yqres.2010.01.004 Published online by Cambridge University Press

Wash in western YPG, which is situated in a similar depositional setting to the sites of this study (Fig. 1). By comparing the sediment yield from historical sediment budgets in Yuma Wash with sediment production rates deduced from isotopic data, an exponential decrease in channel nuclide concentrations with distance downstream is indicated in the basin. Clapp et al. (2002) suggest that as much as 40% of sediment discharged from Yuma Wash is recycled from stored basin alluvium with the remaining sediment sourced largely from colluvium in hollows and along the lower parts of hillslopes under the modern climatic regime. During times of increased stream discharge in the late Holocene, however, fan development reflects considerable increases in sediment yield and channel aggradation relative to the amount of channel deposition that has occurred throughout historical climate.

Alluvial response to climatic variability

Present-day interannual climate variability in the southwestern U.S. is linked to decadal scale changes of sea-surface temperatures (SST) (the Pacific Decadal Oscillation, or PDO), in the form of prolonged dry and wet episodes (Mantua and Hare, 2002). Increases in SST and pressure gradients across the Pacific Ocean promote an El Niño-Southern Oscillation (ENSO) climatic pattern that is commonly reflected in the western U.S. as wetter winters and springs (cool season) associated with low-intensity, long duration north Pacific frontal storm tracks (Cayan et el., 1999). The desert regions of the southwestern U.S. typically receive a much lesser portion of its precipitation during the summer and fall (warm season) by high intensity, short duration convective storms related to moisture surges originating from the Gulf of California that are closely associated with the North American Monsoon (NAM) (Adams and Comrie, 1997; Higgins et al., 2004). The region is also affected by 1–3 eastern Pacific tropical cyclones and their remnants (tropical storms) each year, with individual storms accounting for as much as 95% of the warm-season rainfall, as well as being modulated by ENSO and PDO patterns (e.g., Larson et al., 2005; Corbosiero et al., 2009). The combination of dissipating tropical cyclones and moisture surges also promotes the occurrence of rare mesoscale convective systems, which generate extreme precipitation events over a period of several days that cause widespread landsliding, flooding, and channel erosion (Griffiths et al., 2009).

The frequency and intensity of ENSO variability have increased from the middle to late Holocene, promoting a shift from dryer to wetter conditions, based on model results that are corroborated by marine and terrestrial proxy records (Liu et al., 2000). Terrestrial-based studies in the southwestern U.S. have documented the timing of significant changes in the alluvial and lacustrine records and call upon deviations in the strength and frequency of ENSO variability to help explain temporal patterns. The climatic conditions necessary to explain the widespread alluvial sedimentation, flooding of major river systems, and expansion of lakes are inferred to be related to changes in ENSO patterns. Theses changes are often reflected as an increase in magnitude and frequency of cool-season storms associated with north Pacific frontal storm tracks (Enzel et al., 1989; Ely et al., 1993; Waters and Haynes, 2001; Menking and Anderson, 2003) and warm-season monsoon activity (McDonald et al., 2003; Kirby et al., 2007). It is widely accepted that ENSO variability is responsible for significant landscape changes in the western U.S., although, the timing and types of atmospheric conditions and the character of the hydrologic processes required to create these changes are poorly understood (Scuderi et al., 2010). The Holocene geomorphic record from the Mojave Desert, however, may confirm the occurrence of seasonal partitioning of storm tracks in the arid southwestern U.S. as controlling landscape-process responses to climate forcing. Geomorphic evidence implies that cool-season frontal storms primarily cause flooding of rivers, the expansion of ephemeral lakes, and fan erosion and incision, whereas high intensity, warm-season storms likely cause hillslope erosion and alluvial fan aggradation (Bull, 1991; Miller et al., 2010).

To consider the role of climatic variability and to identify the circulation patterns as drivers of alluvial fan aggradation, precipitation records were compiled from COOP weather stations near Yuma (WRCC, 2009). These stations include Yuma WB City/AP (Fig. 6a), Yuma Proving Ground (Fig. 6b), and Blythe (Fig. 6c), and cover a 100-km transect from south (Yuma WB City/AP) to north (Blythe). The 24-month moving average ENSO (Fig. 6a) and PDO index (Fig. 6b) from Hanson et al. (2004), along with the southern oscillation index (SOI; Fig. 6c) from Redmond and Koch (1991) were then integrated with the precipitation data (e.g., Redmond et al., 2002). This analysis was undertaken to understand the frequency, magnitude, and source of precipitation events necessary to produce the observed late Holocene fan aggradation.

Mean water-year precipitation at these stations ranged from 88.6 to 98.2 mm. All three COOP stations have a significant ($p < 0.05$) correlation for ENSO, PDO, and SOI to both total and non-NAM (October to June) precipitation (Table 3) illustrating the importance of the large-scale, cool-season climatic pattern. Warm-season, NAM precipitation at these stations accounted for 33 to 35% of total precipitation. NAM precipitation, however, is negatively correlated having $r = -0.22$ ($p < 0.05$) at Yuma WB City/AP to the south and positively correlated (although $p > 0.05$) at both YPG with $r = 0.15$ and Blythe having $r = 0.19$ to the north (Table 3). Restricting the data set to years with above average precipitation increased the correlation coefficients (although decreasing the number of records and thus *p value*) between ENSO and non-NAM precipitation at Yuma WB City/AP with $r = 0.48$ ($p = 0.002$), YPG with $r = 0.38$ ($p = 0.11$), and Blythe having $r = 0.26$ ($p = 0.09$), suggesting that the El Niño years (ENSO>1 or SOI < -1) contribute higher total precipitation, whereas NAM cycles are more random.

Extreme precipitation events associated with dissipating tropical cyclones occur during both strong negative SOI (El Niño, SOI < -1) and positive SOI (La Niña, SOI > 1) conditions (Fig. 6). Of the 47 tropical cyclones that occurred in the southwestern U.S. between AD 1933 and 2008 (Corbosiero et al., 2009), 26 produced measurable precipitation at one of these COOP stations with 23% occurring during strong El Niño conditions (SOI < -1), 12% during moderate El Niño ($-1 <$ SOI < -0.5) and 58% occurring during neither El Niño or La Niña ($-0.5 <$ SOI < 0.5). One cyclone (2%) occurred during the transition between moderate and strong La Niña conditions. Many of the largest and intense tropical cyclones/storms to make landfall or that adversely affected the region occurred in the fall prior to or preceding strong El Niño winters (NOAA, 2007).

The highest daily precipitation events in the study area included 160 mm on 31 August AD 1909 at Yuma WB City/AP, 96 mm on 31 October AD 1972 at YPG, and 153 mm on 31 August AD 1989 at Blythe. These storm events were associated with warm-season convective storms related to either NAM or dissipating tropical cyclones that caused severe flooding and erosion, and no significant reactivation of fan surfaces. For perspective, Tropical Storm Nora in AD 1997 made landfall near Yuma from the Gulf of California, and tracked north along the Colorado River valley and western Arizona (Farfn and Zehnder, 2001). Many piedmont slopes within its track were affected by substantial erosion and deposition, but were limited mostly to confined, channelized reaches (Mayer and Pearthree, 2002; Pearthree et al., 2004).

Given the geomorphic and stratigraphic evidence from previous records in the southwestern U.S., it is likely that both frontal and convective atmospheric patterns were intensified during the late Holocene by modulation of ENSO variability. But, the high intensity, short-to-long duration storm events related to dissipating tropical cyclones or mesoscale convective systems most likely produced the large discharges necessary to both widely erode and aggrade sediment. During the late Holocene, these storm events and related large increases in sediment discharge created the alluvial cut-and-fill

https://doi.org/10.1016/j.yqres.2010.01.004 Published online by Cambridge University Press

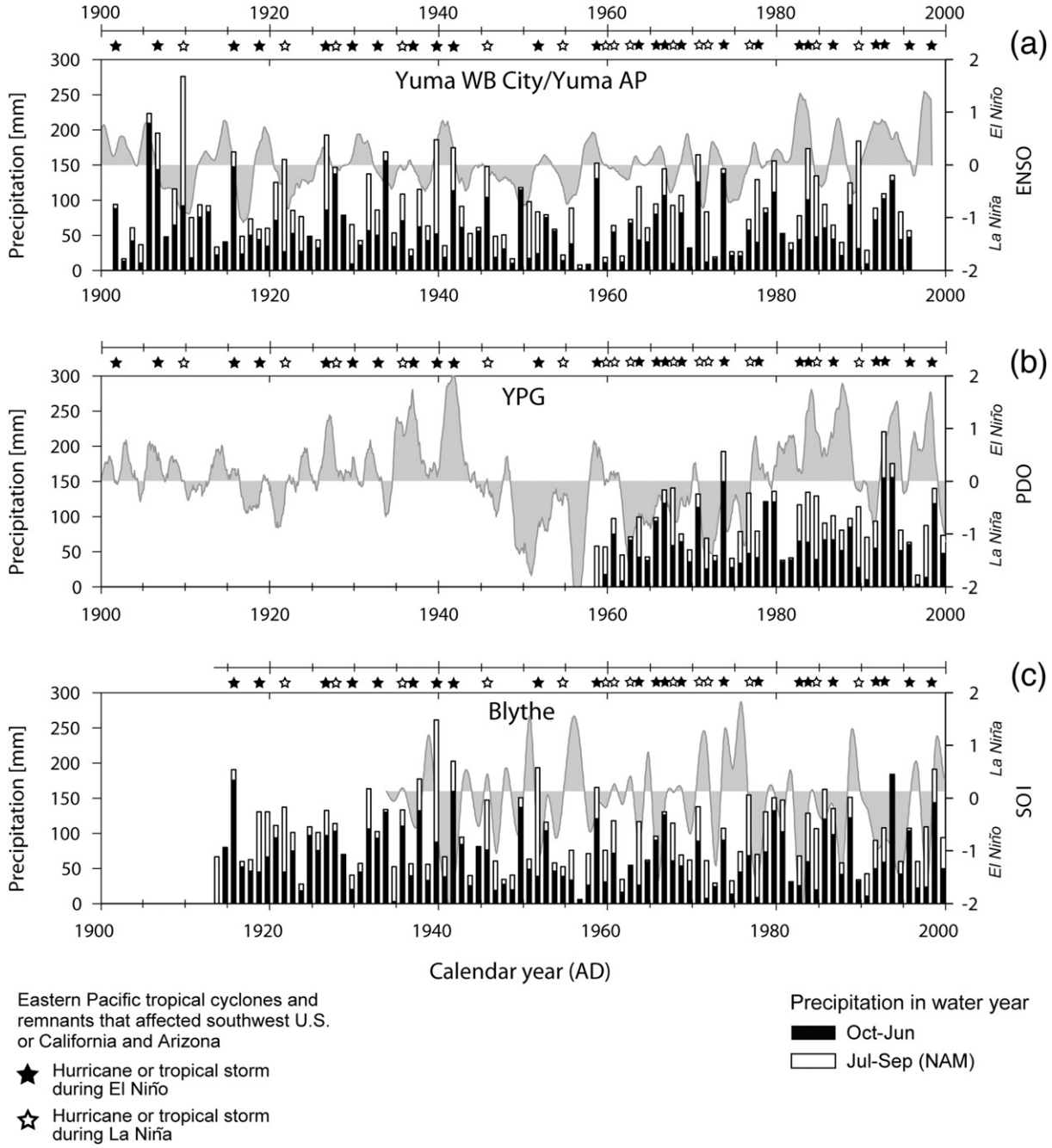

Figure 6. (a) Precipitation between AD 1900 and 1994 from Yuma WB City/Yuma Airport weather station (COOP ID 029662 and 029660) (left side scale) plotted against the 24-month moving average El Niño-Southern Oscillation (ENSO) from Hanson et al. (2004) (right side scale). (b) Precipitation between AD 1958 to 1998 from Yuma Proving Ground weather station (COOP ID 029654) (left side scale) plotted against the 24-month moving average Pacific Decadal Oscillation (PDO) from Hanson et al. (2004) (right side scale). (c) Precipitation between AD 1913 to 1998 from Blythe COOP weather station (COOP ID 040924) (left side scale) plotted against the 24-month moving average Southern Oscillation Index (SOI) from Redmond and Koch (1991) (right side scale). Annual precipitation by water year is partitioned between the cool-season (October to June) and warm-season (July to September) and shown with black and white histograms, respectively. ENSO, PDO, and SOI are shown by gray backgrounds. Colored stars signify eastern Pacific tropical cyclones and remnants that affected the southwestern U.S. either during El Niño or La Niña conditions. Information on the dates of specific tropical cyclones (i.e., hurricanes or tropical storms) between AD 1900 and 1957 is from NOAA (2007) and between AD 1958 and 1999 is from Corbosiero et al. (2009). NAM, North American Monsoon.

deposits and well-sorted fluvial sedimentology observed near Yuma. The magnitude of this discharge is unmatched in the ~100 yr historical record of storm events and sedimentation.

Timing of late Holocene ENSO variability from paleoclimate proxies

Climate variability in the Holocene is reflected differently across the globe and is represented by six intervals of significant rapid climate change between 9000–8000, 6000–5000, 4200–3800, 3500–2500, 1200–1000, and 600–150 cal yr BP (Mayewski et al., 2004). In the southwestern U.S., the time period from 4200 and 3800 cal yr BP represents a change from warm and dry climate to cool and wet conditions, according to numerous terrestrial paleoclimatic proxy records in California (e.g., Malamud-Roam et al., 2006), vegetation records from the Mojave and Sonoran Deserts (e.g., McAuliffe and Van Devender, 1998; Koehler et al., 2005), as well as marine sediment records from the Santa Barbara Basin off southern California (Friddell et al., 2003). The 900 yr period of alluvial aggradation near Yuma, 3200 to 2300 cal yr BP, occurred during a time of rapid global climate change between 3500 and 2500 cal yr BP

https://doi.org/10.1016/j.yqres.2010.01.004 Published online by Cambridge University Press

Table 3
Pearson product moment correlation coefficients between large-scale climate circulation indices of El Niño (ENSO), Pacific decadal oscillation (PDO), and southern oscillation index (SOI) to total, North American monsoon (NAM; June to September) and the remainder of water-year precipitation from COOP stations at Yuma WB City/AP, the Yuma Proving Ground (YPG) in AZ and Blythe, CA.

		ENSO	PDO	SOI	Yuma WB City/AP			YPG			Blythe		
					Total	NAM	Other	Total	NAM	Other	Total	NAM	Other
	ENSO	1											
	PDO	0.53^{2**}	1										
	SOI	-0.50^{1**}	-0.46^{2**}	1									
	Total	0.23^{1*}	0.23^{5*}	−0.34*	1								
Yuma WB City/AP	NAM	-0.22^{11*}	0.1	0.09	0.65**	1							
	Other	0.33^{2**}	0.26^{6*}	−0.52**	0.75**	−0.01	1						
	Total	0.33^{2*}	0.2	−0.35*	0.69**	0.2	0.70**	1					
YPG	NAM	0.15	0.12	0.22	0.32*	0.59**	−0.11	0.43**	1				
	Other	0.31^{2*}	0.15	−0.53**	0.56**	−0.18	0.89**	0.81**	−0.19	1			
	Total	0.31^{2*}	0.28^{4*}	−0.24*	0.66**	0.28*	0.61**	0.59**	0.05	0.63**	1		
Blythe	NAM	0.19	0.13	0.24*	0.26*	0.48**	−0.08	0.21	0.60**	−0.15	0.54**	1	
	Other	0.31^{1*}	0.33^{2*}	−0.48**	0.57**	−0.05	0.78**	0.48*	−0.3	0.75**	0.77**	−0.11	1

*$P<0.05$, **$P<0.001$; ENSO and PDO superscript indicate the monthly time series of highest correlation (e.g., 1 = January), data from Hanson et al. (2004); SOI from Redmond and Koch (1991); total = water year precipitation, NAM (July–September), and other (October–June).

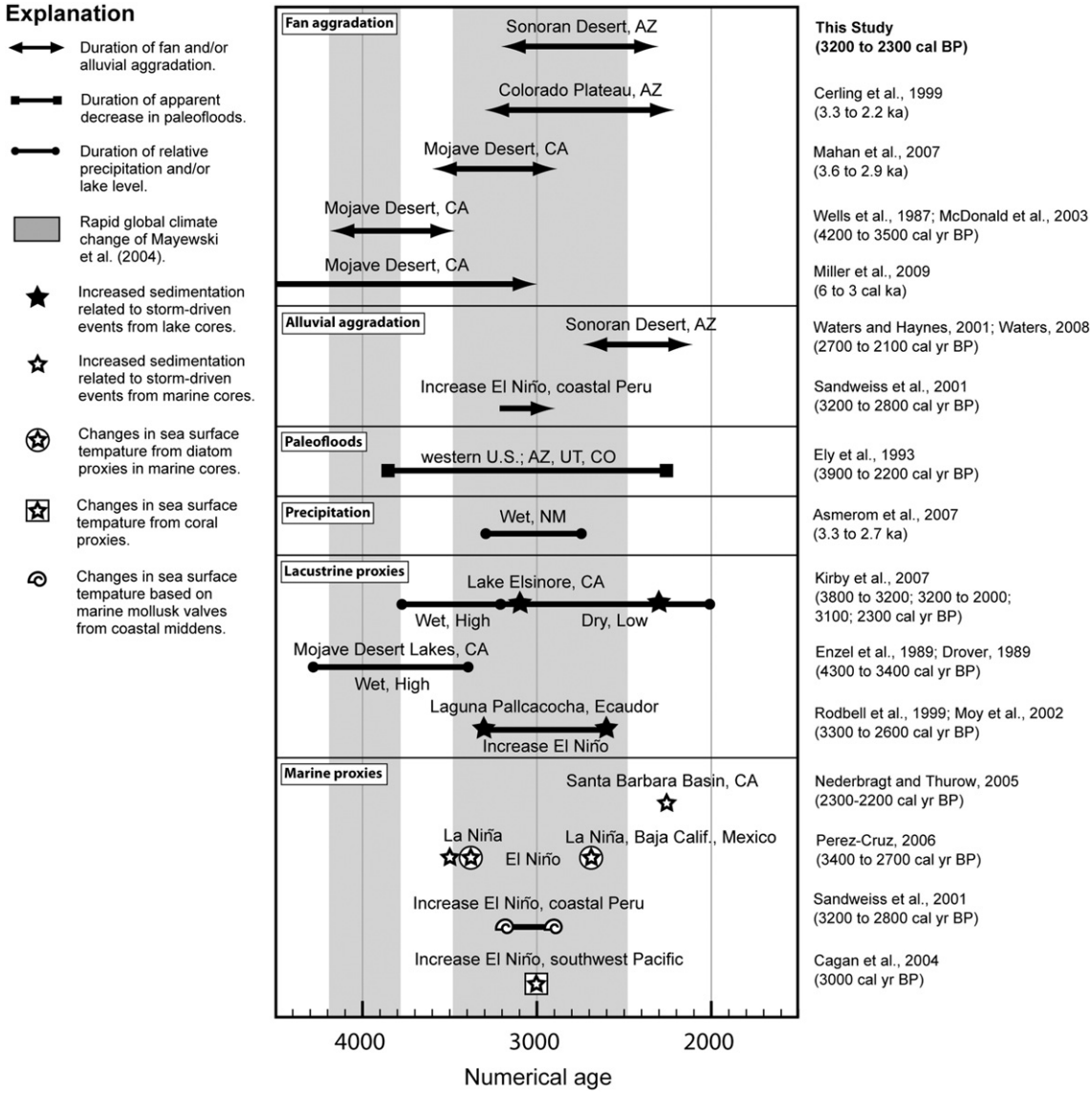

Figure 7. Compilation of geomorphic, archeological, and sediment core data depicting a wide range of paleoclimate proxy data sets from the southwestern U.S., Mexico, South America, and southwest Pacific that span the interval of rapid climate change between 3500 and 2500 yr ago.

https://doi.org/10.1016/j.yqres.2010.01.004 Published online by Cambridge University Press

(Fig. 7). Geologic-based paleoclimatic proxy records from a wide range of well-dated records also indicate an increase in effective moisture and regional alluvial aggradation and flooding during this later period (Fig. 7).

Paleoflood chronology of large watersheds in the western U.S. shows a distinct period of numerous region-wide floods from ~5600 to 3900 cal yr BP, followed by a period from ~3900 to 2200 cal yr BP with sharply reduced flooding (Ely et al., 1993). Although region-wide flooding of large river systems decreased from 3.9 to 2.2 ka, other proxy records indicate unusually wet conditions occurred across the western U.S. during this period. For example, increased precipitation in New Mexico started at ~3.3 ka and in particular at 2.7 ka, based on ^{230}Th-^{234}U dating of speleothems (Asmerom et al., 2007). Additional alluvial records show arroyo cutting-and-filling cycles in several valleys of the upper Gila River drainage basin in Arizona increased dramatically after 4600–4300 cal yr BP with two distinct episodes of arroyo cutting and vertical aggradation of flood plain deposits at 2700–2400 cal yr BP and ~2100 cal yr BP (Waters and Haynes, 2001; Waters, 2008). Northern Arizona also records episodes of alluvial aggradation at ~3.3 ka and again at 2.2 ka based on cosmogenic ^{3}He ages from the largest debris flow fan in the Grand Canyon (Cerling et al., 1999). Alluvial systems aggraded all across the Colorado Plateau and northern Sonoran Desert at the same time as aggradation in the Mojave Desert. Alluvial fans within the Mojave Desert regionally aggraded between ~6 and 3 cal ka (Mahan et al., 2007; Miller et al., 2010), and in the Soda and Providence Mountains from 4200 to 3500 cal yr BP (Wells et al., 1987; McDonald et al., 2003).

The lacustrine sediment core record from Lake Elsinore in southern California offers additional insight to climate variability during this period by showing relative high lake levels (wet, variable climate) from 3800 to 3200 cal yr BP and relative low lake levels (dry, less variable climate) from 3200 to 2000 cal yr BP. In addition, two discrete intervals in the record contain high concentrations of thin silt layers likely related to increases in storm events dated at ~3100 cal yr BP and ~2300 cal yr BP (Kirby et al., 2004; 2007) (Fig. 7). East of Lake Elsinore in the Mojave Desert, lakes expanded on playas for periods of years to decades. Here, sediment records indicate shallow lakes expanded at Silver Lake playa from 4200–3700 cal yr BP (Enzel et al., 1989) and at Cronese Lake from 4300–3400 cal yr BP (Drover, 1987). In addition to the lacustrine records, a marine sediment core record from Santa Barbara Basin revealed six continuous intervals of terrigenous laminae representing an increase in ENSO-related rainfall and river runoff in the past 15,000 yr with one of the intervals dated at ~2300–2200 cal yr BP (Nederbragt and Thurow, 2005).

Other paleoclimatic proxy records display ENSO variability outside the western U.S. during this same period of rapid global climate change. Marine paleoclimatic proxies from sediment cores in the Gulf of California near La Paz, Baja California, Mexico indicate two significant ocean cooling conditions centered at 3400 cal yr BP and 2700 cal yr BP, which are the two more pronounced late Holocene events identified in the record (Fig. 7). The two cooling events bound a 700 yr period of elevated ocean temperatures characteristic of ENSO type sea-surface conditions, as well as spikes in magnetic susceptibility attributed to an increase in terrigenous input related to local stream runoff (Prez-Cruz, 2006). The timing of specific ENSO sea-surface conditions near La Paz, is also similar to marine paleoclimatic evidence from the Guaymas Basin, Gulf of California, Mexico (Barron et al., 2005). In South America, the lacustrine record from Laguna Pallcacocha in southern Ecuador, which is strongly influenced by ENSO variability, shows one of the more extensively laminated intervals in the record from 3300 to 2600 cal yr BP that is attributed to ENSO-driven alluvial deposition in the drainage basin (Rodbell et al., 1999; Moy et al., 2002) (Fig. 7). The lacustrine proxy record in southern Ecuador is supported by the analysis of marine mollusks from archeological sites in Peru that indicate an increase in frequency of El Niño variability after 3200–2800 cal yr BP (Sandweiss et al., 2001). The alluvial flood plain stratigraphy in northern coastal Peru also shows a similar result with an increase in frequency and magnitude of flooding in the region attributed to El Nio-driven events starting at 3200 cal yr BP (Wells, 1990). The overall timing of the intensification of ENSO variability during this specific period of rapid climate change is also reflected in paleoclimatic proxy records from the Equatorial Pacific Ocean associated with the Indo-Pacific Warm Pool. Here, modern ENSO periodicities began ~5 ka with an abrupt increase in ENSO magnitude occurring ~3 ka based on coral records (Gagan et al., 2004) (Fig. 7).

Conclusions

A variety of supporting evidence from paleoclimatic proxy records correlates well with each other, and collectively demonstrates an abrupt increase in climate variability from ~3300 to 2300 cal yr BP. In the western U.S., the climate variability is reflected as enhanced effective moisture associated with an increase in frequency and intensity of ENSO patterns. Alluvial fan aggradation near Yuma between 3200 and 2300 cal yr BP coincides with this period of climate change. The atmospheric conditions necessary for the regional alluvial aggradation and fluvial-type sedimentology are likely related to frequently occurring periods (decades to centuries) of extreme storm events associated with the onset of an intensified ENSO cycle at ~3300 cal yr BP. If the atmospheric circulation patterns at this time were similar to historical climate, a greater frequency of high-intensity, warm-season storms related to dissipating tropical cyclones and mesoscale convective systems are the probable causes of the alluvial fan aggradation. While we cannot preclude the influence of enhanced cool-season, north Pacific frontal storms in also contributing moisture to the region over this ~900 yr period, it is possible that both seasonal climatic patterns are required to cause alluvial aggradation at scales not represented in the historical record.

Acknowledgments

The authors acknowledge G. Stullenbarger and W. Lucas of YPG-Natural Environments Testing Office (NETO) for logistical support and R.T. Hanson for the 100-yr ENSO data set. We thank D. Rhode and D. Sada for guidance in the identification of wood and snail samples, respectively, and T. Bullard for discussions on extreme storm events and alluvial fan response. We also thank two anonymous reviewers and the editors of *QR* for their comments, which strengthened the manuscript. This project was partially funded by YPG-NETO (W9124R-07-C-0028/CLIN 0001-ACRN-AA) and the Army Research Office (DAAD19-03-1-0159).

References

Adams, D.K., Comrie, A.C., 1997. The North American Monsoon. Bulletin of the American Meteorological Society 78, 2197–2213.
Asmerom, Y., Polyak, V., Burns, S., Rassmussen, J., 2007. Solar forcing of Holocene climate: New insights from a speleothem record, southwestern United States. Geology 35, 1–4.
Bacon, S.N., McDonald, E.V., Baker, S.E., Caldwell, T.G., Stullenbarger, G., 2008. Desert terrain characterization of landforms and surface materials within vehicle test courses at U.S. Army Yuma Proving Ground, USA. Journal of Terramechanics 45, 167–183.
Barron, J.A., Bukry, D., Dean, W.E., 2005. Paleoceanographic history of the Guaymas Basin, Gulf of California, during the past 15,000 years based on diatoms, silicoflagellates, and biogenic sediments. Marine Micropaleontology 56, 81–102.
Bequaert, J.C., Miller, W.B., 1973. The Mollusks of the Arid Southwest; with an Arizona Check List. University of Arizona Press, Tuscon, Arizona, p. 271.
Birkeland, P.W., 1999. Soils and Geomorphology, 3rd ed. Oxford Univ. Press, New York, p. 372.

https://doi.org/10.1016/j.yqres.2010.01.004 Published online by Cambridge University Press

Brennan, R., Quade, J., 1997. Reliable Late-Pleistocene stratigraphic ages and shorter groundwater travel times from ^{14}C in fossil snail from the southern Great Basin. Quaternary Research 47, 329–336.
Bull, W.B., 1991. Geomorphic Responses to Climate Change. Oxford Univ. Press, New York, p. 326.
Cayan, D.R., Redmond, K.T., Riddle, L.G., 1999. ENSO and hydrologic extremes in the western United States. Journal of Climate 2, 2881–2893.
Cerling, T.E., Webb, R.H., Poreda, R.J., Rigby, A.D., Melis, T.S., 1999. Cosmogenic ^{3}He and frequency of late Holocene debris flows from Prospect Canyon, Grand Canyon, USA. Geomorphology 27, 93–111.
Clapp, E.M., Bierman, P.R., Caffee, M., 2002. Using ^{10}Be and ^{26}Al to determine sediment generation rates and identify sediment source areas in an arid region drainage basin. Geomorphology 45, 89–104.
Cochran, C.C., 1991. Soil survey of the U.S. Army Yuma Proving Ground, Arizona—parts of La Paz and Yuma Counties. U.S. Department of Agriculture, Natural Resources Conservation Services Soil Survey Report, 164 p, 1:24,000.
Corbosiero, K.L., Dickinson, M.J., Bosart, LF., 2009. The contribution of eastern North Pacific tropical cyclones to the rainfall climatology of the southwest United States. Monthly Weather Review 137, 2415–2435.
Donders, T.H., Wagner-Cremer, F., Visscher, H., 2008. Integration of proxy data and model scenarios for the mid-Holocene onset of modern ENSO variability. Quaternary Science Reviews 27, 571–579.
Dreimanis, A., 1962. Quantitative gasometric determinations of calcite and dolomite by using Chittick apparatus. Journal of Sedimentary Petrology 32, 520–529.
Drover, C.E., 1987. The Early Prehistoric Ecology of the Northern Mojave Sink. San Bernardino County, California. Unpubl. PhD dissertation. Univ. of Califonria, Riverside, p. 255.
Ely, L.L., Enzel, Y., Baker, V.R., Cayan, D.R., 1993. A 5000-year record of extreme floods and climate change in the southwestern United States. Science 262, 410–412.
Enzel, Y., Cayan, D.R., Anderson, R.Y., Wells, S.G., 1989. Atmospheric circulation during Holocene lake stands in the Mojave Desert: evidence for regional climatic change. Nature 341, 44–47.
Farfn, L.M., Zehnder, J.A., 2001. An analysis of the landfall of Hurricane Nora (1997). Monthly Weather Review 129, 2073–2088.
Friddell, J.E., Thunell, R.C., Guilderson, T.P., Kashgarian, M., 2003. Increased northeast Pacific climatic variability during the warm middle Holocene. Geophysical Research Letters 30 (11), 1560, doi:10.1029/2002GL016834.
Gagan, M.K., Hendy, E.J., Haberle, S.G., Hantoro, W.S., 2004. Post-glacial evolution of the Indo-Pacific Warm Pool and El Niño-Southern oscillation. Quaternary International 118–119, 127–143.
Gee, G.W., Or, D., 2002. Particle-size analysis. In: Dane, J.H., Topp, G.C. (Eds.), Methods of Soil Analysis, Part 4. Physical Methods, Soil Science Society of America Book Series 5, pp. 255–293.
Griffiths, P.G., Magirl, C.S., Webb, R.H., Pytlak, E., Troch, P.A., Lyon, S.W., 2009. Spatial distribution and frequency of precipitation during an extreme event: July 2006 mesoscale convective complexes and floods in southeastern Arizona.
Hanson, R.T., Newhouse, M.W., Dettinger, M.D., 2004. A methodology to assess relations between climatic variability and variations in hydrologic time series in the southwestern United States. Journal of Hydrology 287, 252–269.
Higgins, R.W., Shi, W., Hain, C., 2004. Relationships between Gulf of California moisture surges and precipitation in the southwestern United States. Journal of Climate 17, 2983–2997.
House, P.K., Pearthree, P.A., Perkins, M.E., 2008. Stratigraphic evidence for the role of lake spillover in the inception of the lower Colorado River in southern Nevada and western Arizona. In: Reheis, M.C., Hershler, R., Miller, D.M. (Eds.), Late Cenozoic Drainage History of the Southwestern Great Basin and Lower Colorado River Region: Geologic and Biotic Perspectives, 439. Geological Society of America Special Paper, pp. 335–353.
Kirby, M.E., Poulsen, C.J., Lund, S.P., Patterson, W.P., Reidy, L., Hammond, D.E., 2004. Late Holocene lake level dynamics inferred from magnetic susceptibility and stable oxygen isotope data: Lake Elsinore, southern California (USA). Journal of Paleolimnology 31, 275–293.
Kirby, M.E., Lund, S.P., Anderson, M.A., Bird, B.W., 2007. Insolation forcing of Holocene climate change in southern California: a sediment study from Lake Elsinore. Journal of Paleolimnology 38, 395–417.
Koehler, P.A., Anderson, R.S., Spaulding, W.G., 2005. Development of vegetation in the central Mojave Desert of California during the late Quaternary. Paleogeography, Paleoclimatology, Paleoecology 215, 297–311.
Larson, J., Zhou, Y., Higgins, R.W., 2005. Characteristics of landfalling tropical cyclones in the United States and Mexico: Climatology and interannual variability. Journal of Climate 18, 1247–1262.
Lashlee, D., Briuer, F., Murphy, W., McDonald, E.V., 2001. Geomorphic mapping enhances cultural resources management at the U.S. Army Yuma Proving Ground, Arizona, USA. Arid Land Research and Management 16, 213–229.
Liu, Z., Kutzbach, J., Wu, L., 2000. Modeling climate shift of El Niño variability in the Holocene. Geophysical Research Letters 27, 2265–2268.
Machette, M.N., 1985. Calcic soils of the southwestern United States. In: Weide, D. (Ed.), Soils and Quaternary Geology of Southwestern United States, 203. Geological Society of America Special Paper, pp. 1–21.
Mahan, S.A., Miller, D.M., Menges, C.M., Yount, J.C., 2007. Late Quaternary stratigraphy and luminescence geochronology of the northeastern Mojave Desert. Quaternary International 166, 61–78.
Malamud-Roam, F.P., Ingram, B.L., Hughes, M., Florsheim, J.L., 2006. Holocene paleoclimate records from a large California estuarine system and its watershed region: linking watershed climate and bay conditions. Quaternary Science Reviews 25, 1570–1598.
Mantua, N.J., Hare, S.R., 2002. The Pacific decadal oscillation. Journal of Oceanography 58, 35–42.
Mayer, L., Pearthree, P.A., 2002. Mapping flood inundation in southwestern Arizona using Landsat TM Data: a method for rapid regional flood assessment following large storms. In: House, P.K., Webb, R.H., Baker, V.R., Levish, D.R. (Eds.), Ancient Floods, Modern Hazards; Principles and Applications of Paleoflood Hydrology, Water Science and Application No. 5. American Geophysical Union, pp. 61–76.
Mayewski, P.A., Rohling, E.E., Stager, J.C., Karlen, W., Maasch, K.A., Meeker, L.D., Meyerson, E.A., Gasse, F., van Kreveld, S., Holmgren, K., Lee-Thorp, J., Rosqvist, G., Rack, F., Staubwasser, M., Schneider, R.R., Steig, E.J., 2004. Holocene climate variability. Quaternary Research 62, 243–255.
McAuliffe, J.R., McDonald, E.V., 2006. Holocene environmental change and vegetation contraction in the Sonoran Desert. Quaternary Research 65, 204–215.
McAuliffe, J.R., Van Devender, T.R., 1998. A 22,000-year record of vegetation change in the north-central Sonoran Desert. Paleogeography, Paleoclimatology, Paleoecology 141, 253–275.
McDonald, E.V., McFadden, L.D., Wells, S.G., 2003. Regional response of alluvial fans to the Pleistocene-Holocene climatic transition, Mojave Desert, California. In: Enzel, Y., Wells, S.G., Lancaster, N. (Eds.), Paleoenvironments and Paleohydrology of the Mojave and Southern Great Basin Deserts, 368. Geological Society of America Special Paper, pp. 189–205.
McFadden, L.D., Ritter, J.B., Wells, S.G., 1989. Use of multiparameter relative-age methods for age estimation and correlation of alluvial-fan surfaces on a desert piedmont, eastern Mojave Desert. California. Quaternary Research 32, 276–290.
McFadden, L.D., McDonald, E.V., Wells, S.G., Anderson, K., Quade, J., Forman, S.L., 1998. The vesicular layer and carbonate collars of desert soils and pavements: formation, age and relation to climate change. Geomorphology 24, 101–145.
Menking, K.M., Anderson, R.Y., 2003. Contributions of La Niña and El Niño to middle Holocene drought and late Holocene moisture in the American Southwest. Geology 31, 937–940.
Miller, D.M., Schmidt, K.M., Mahan, S.A., McGeehin, J.P., Owen, L.A., Barron, J.A., Lehmkuhl, F., 2010. Holocene landscape response to seasonality of storms in the Mojave Desert. Quaternary International 215, 45–61.
Moy, C.M., Seltzer, G.O., Rodbell, D.T., Anderson, D.M., 2002. Variability of El Niño/southern oscillation activity at millennial timescales during the Holocene epoch. Nature 420, 162–165.
Nederbragt, A.J., Thurow, J., 2005. Amplitude of ENSO cycles in the Santa Barbara Basin, off California, during the past 15000 years. Journal of Quaternary Science 20, 447–456.
Nichols, K.K., Bierman, P.R., Ross Foniri, W., Gillespie, A.R., Caffee, M., Finkel, R., 2006. Dates and rates of arid region geomorphic processes. GSA Today 16, 4–11.
NOAA [National Oceanic and Atmospheric Administration], 2007. A history of significant weather events in southern California. Report prepared by the National Weather Service in San Diego 91.
Olmsted, F.H., 1972. Geologic map of the Laguna Dam 7.5-minute quadrangle, Arizona and California. U.S. Geological Survey Geologic Quadrangle Map GQ-1014, 1:24,000.
Pearthree, P.A., Klawon, J.E., and Lehman, T.W., 2004. Geomorphology and hydrology of an alluvial fan flood on Tiger Wash, Maricopa and La Paz Counties, west-central Arizona, Arizona Geological Survey OFR-04-02, 40 p., 2 sheets on CD-ROM, scale 1:24,000.
Prez-Cruz, L., 2006. Climate and ocean variability during the middle and late Holocene recorded in laminated sediments from Alfonso Basin, Gulf of California, Mexico. Quaternary Research 65, 401–410.
Peterson, F.F., 1981. Landforms of the Basin and Range province: defined for soil survey. Nevada agriculture experiment station, University of Nevada, Reno, Technical Bulletin 28, 52 p.
Pigati, J.S., Quade, J., Shahanan, T.M., Haynes, C.V., 2004. Radiocarbon dating of minute gastropods and new constraints on the timing of late Quaternary spring-discharge deposits in southern Arizona, USA. Paleogeography, Paleoclimatology, Paleoecology 204, 33–45.
Redmond, K.T., Koch, R.W., 1991. Surface climate and streamflow variability in the Western United States and their relationship to large-scale circulation indexes. Water Resources Research 27, 2381–2399.
Redmond, K.T., Enzel, Y., House, P.K., Biondi, F., 2002. Climate variability and flood frequency at decadal to millennial time scales. In: House, P.K., Webb, R.H., Baker, V.R., Levish, D.R. (Eds.), Ancient Floods, Modern Hazards; Principles and Applications of Paleoflood Hydrology, Water Science and Application No. 5. American Geophysical Union, pp. 21–45.
Reheis, M.C., Goodmacher, J.C., Harden, J.W., McFadden, L.D., Rockwell, T.K., Shroba, R.R., Sowers, J.M., Taylor, E.M., 1995. Quaternary soils and dust deposition in southern Nevada and California. Geological Society of America Bulletin 107, 1003–1022.
Reimer, P.J., Baillie, M.G.L., Bard, E., Bayliss, A., Beck, J.W., Bertrand, C.P., Blackwell, G., Buck, C.E., Burr, G., Cutler, K.B., Damon, P.E., Edwards, R.L., Fairbanks, R.G., Friedrich, M., Guilderson, T.P., Hughen, K.A., Kromer, B.F., McCormac, G., Manning, S., Bronk Ramsey, C., Reimer, R.W., Remmele, S., Southon, J.R., Stuiver, M., Talamo, S., Taylor, F.W., van der Plicht, J., Weyhenmeyer, C.E., 2004. IntCal04 terrestrial radiocarbon age calibration, 0-26 cal Kyr BP. Radiocarbon 46, 1029–1058.
Rhoades, J.D., 1996. Salinity: electrical conductivity and total dissolved solids. In: Sparks, D.L. (Ed.), Methods of Soil Analysis, Part 3: Chemical Methods, Monograph No. 5. American Society of Agronomy, Madison, WI, pp. 417–435.
Richard, S.M., Reynolds, S.J., Spencer, J.E., and Pearthree, P.A., comps., 2000. Geologic map of Arizona: Arizona Geological Survey Map M-35, 1 sheet, scale: 1:1,000,000.

Ritter, J.B., Miller, J.R., Husek-Wulforst, J., 2000. Environmental controls on the evolution of alluvial fans in Buena Vista Valley, North Central Nevada, during late Quaternary time. Geomorphology 36, 63–87.
Rodbell, D.T., Seltzer, G.O., Anderson, D.M., Abbott, M.B., Enfield, D.B., Newman, J.H., 1999. An ~15,000-year record of El Niño-driven alluviation in southwestern Ecuador. Science 283, 516–520.
Sandweiss, D.H., Maasch, K.A., Burger, R.L., Richardson, J.B., Rollins, H.B., Clement, A., 2001. Variation in Holocene El Niño frequencies: climate records and cultural consequences in ancient Peru. Geology 29, 603–606.
Schoeneberger, P.J., Wysocki, D.A., Benham, E.C., Broderson, W.D., 2002. Field Book for Describing and Sampling Soils, Version 2.0. Natural Resources Conservation Service, National Soil Survey Center, Lincoln, NE.
Scuderi, L.A., Laudadio, C.K., Fawcett, P.J., 2010. Monitoring playa lake inundation in the western United States: Modern analogues to late-Holocene lake level change. Quaternary Research 73, 48–58.
Soil Survey Staff, 1998. Keys to Soil Taxonomy, 8th ed. USDA, Natural Resources Conservation Service, U.S. Government Printing Office, Washington, D.C., p. 326.
Stuiver, M., Reimer, P., 1993. Extended 14C databases and revised CALIB radiocarbon calibration program. Radiocarbon 28, 1022–1030.
Waters, M.R., 2008. Alluvial chronologies and archaeology of the Gila River drainage basin. Arizona. Geomorphology 101, 332–341.
Waters, M.R., Haynes, C.V., 2001. Late Quaternary arroyo formation and climate change in the American southwest. Geology 29, 399–402.
Wells, L.E., 1990. Holocene history of the El Niño phenomenon as recorded in flood sediments of northern coastal Peru. Geology 18, 1134–1137.
Wells, S.G., McFadden, L.D., Dohrenwend, J.C., 1987. Influence of late Quaternary climatic changes on geomorphic and pedogenic processes on a desert piedmont, eastern Mojave Desert. California. Quaternary Research 27, 130–146.
Wilshire, H.G., Reneau, S.L., 1992. Geomorphic surfaces and underlying deposits of the Mojave Mountains Piedmont, Lower Colorado River, Arizona. Zeitschrift fur Geomorphologie 36, 207–226.
WRRC [Western Regional Climate Center], 2009. Historical precipitation information. http://www.wrcc.dri.edu/CLIMATEDATA.html.